Novel Meshing Stiffness Model for Spur Gear Pairs Considering the Temperature Effect

Yanbing HE*, Haibo YANG***,****

**School of Mechanical Engineering, University of Science and Technology Beijing, Beijing 100083, China,
E-mail: hyb20222022@163.com (Corresponding author)*
**Jiangxi Consulting & Investment Group Co., Ltd., Nanchang 330046, China
****School of Mechanical Engineering, University of Science and Technology Beijing, Beijing 100083, China;
E-mail: yhb@ustb.edu.cn*
****Dongguan Institute of Materials and Genes Advanced Institute of Technology, Dongguan 523808, China

1. Introduction

Gear stiffness lays a foundation for studying the dynamic performance of gear transmission systems. In recent years, scholars have conducted extensive studies on gear stiffness based on methods, such as analytical [1-6], finite element [7-11], and experimental research methods [12-13]. Based on the integral potential energy method a novel analytical method for accurately determining the spur gears mesh stiffness was proposed by Tang et al. [4]. An improved method to calculate the helical gear's meshing stiffness was propsoed based on the slicing method in literature [5]. Yang et al. [6] used the parametric equations for a flank profile. The analytical formulations for the time-varying meshing stiffness (TVMS) of a spur gear considering the actual tooth profile geometry were derived. The meshing stiffness of an asymmetric tooth was obtained by using the finite element method (FEM) in literature [10]. Gooley et al. [11] predicted the meshing stiffness of gears by using FEM. Raghuwanshi et al. [13] used the laser displacement sensor technique to measure the meshing stiffness of gears. In addition, numerous scholars have investigated the factors influencing gear stiffness for a more accurate measurement of the gear meshing stiffness. These include spalling defects, cracks, tooth profile shifts, tooth pitting, and temperature. Saxena et al. [14], Ma et al. [15], and Cui et al. [16] investigated the influence of spalling defects on the gear meshing stiffness. The calculation method for the gear's meshing stiffness with spalling defects was developed. Based on this, Luo et al. [17] proposed a new method to calculate the TVMS of gears with curved-bottom features with tooth spalls. Wang et al. [18] investigated the effect of cracks and complex foundations on the gear meshing stiffness. Jiang et al. [19-20] studied the effect of cracks on the gear meshing stiffness and considered the influence of the gear body deflection caused by tooth cracks. Chen et al. [21] investigated the effect of non-uniformly distributed tooth root cracks on the meshing stiffness of gears. Moreover, the effects of a tooth profile shift, pitting, lubrication, and axial force on gear meshing stiffness were investigated by Chen et al. [22], Liang et al. [23], Cheng et al. [24], and Wang et al. [25], respectively. In terms of temperature factors, Gou et al. [26] established a mathematical expression for the deformation of tooth profile owing to the tooth surface contact temperature. Following this, they studied the effect of the contact temperature on the gear meshing stiffness in accordance

with the Hertz contact theory. The concept of thermal stiffness of gears was proposed in literature [27]. In addition, a semi-analytical method for determining the thermal stiffness of spur gears was provided by introducing a correction coefficient, which was verified using the FEM. Lin et al. [28] proposed an analytic algorithm for the meshing stiffness of helical gears considering the temperature effect based on the slice method and potential energy method. To summarize, certain achievements have been made in the study of the influence of temperature on gear stiffness. However, the calculations involved in the FEM remain complex. The semi-analytical method based on the correction coefficient is not universal. Moreover, all the above studies have been conducted under the thermal expansion condition. Therefore, the temperature meshing stiffness of the gear pair was investigated in the full temperature range in this study. The research results can provide a theoretical basis for conducting accurate dynamic studies on gear transmission systems over a wide temperature range (such as the high-speed railway from Northeast to Guangdong), which is a significant contribution to the existing literature.

The remainder of this paper is organized as follows. Section 1 defines the temperature stiffness of a gear pair. In Section 2, the temperature stiffness model is established based on the conservation of energy. Thereafter, the general formulation for calculating the temperature meshing stiffness of the gear pair in the full temperature range is derived. In Section 3, the numerical calculation and discussion are presented. The influence of the tooth profile shift and temperature distribution on the tooth surface on the temperature stiffness is discussed. In Section 4, an indirect experimental verification is presented. Finally, Section 5 presents the main conclusions of this study.

2. Definition of temperature stiffness

In the process of gear meshing, the thermal expansion of gear teeth caused by friction heat from the meshing tooth surface influences the stiffness of the gear. In [27], the influence of heat on gear stiffness was studied, and the definition and calculation method for gear thermal stiffness were presented. However, the standard state of a gear corresponds to a standard temperature owing to the expansion and contraction of the material. A gear contracts when the gear temperature below the standard temperature, and expands when the gear temperature is higher than the standard

temperature. In this study, the concept of gear thermal stiffness is extended to the full temperature range to investigate the effects of expansion with heat and contraction with cold on the gear stiffness. The temperature stiffness of gears can be defined as Eq. (1):

$$c = \frac{F_n}{\Delta_n},$$ (1)

where: F_n denotes the normal external load of the gear; c is the temperature stiffness of the gear; Δ_n is the coupling deformation along the line of action, which considers the influence of temperature.

3. Temperature stiffness based on energy conservation

According to Eq. (1), the key to calculate c is to identify a method to evaluate Δ_n. In this study, a temperature stiffness model was established based on energy conservation. Thereafter, the temperature stiffness was studied under the conditions of expansion and contraction.

3.1. Temperature stiffness in thermal expansion state

Under the tooth thermal expansion condition, the thermal expansion is restricted at the contact point. Furthermore, the directions of tooth profile expansion and the elastic deformation caused by the external load are opposite. An additional thermal load and thermal deformation are generated. This affects the gear's stiffness. In this study, the energy conservation method was employed to establish the spur gear pair's temperature stiffness model under the condition of thermal expansion (Fig. 1). In the proposed model, the gear is fixed, and the pinion can slide in the grooves without friction. The gear and pinion are connected by two compression springs and an extension spring. An air cylinder is mounted between the two compression springs. In Fig. 1, s, s_1 and s_2 are the stiffness of the extension spring, first compression spring, and second compression spring, respectively. These also indicate the standard meshing stiffness k of the tooth pair, single-tooth standard stiffness k_1 of the pinion, and single-tooth standard stiffness k_2 of the gear. That is, $s=k$, $s_1=k_1$, and $s_2=k_2$. For the convenience of description, the symbol k, k_1, and k_2 are used uniformly in the subsequent sections.

In the standard state, the extension spring has its original length, x_0. Thus, no deformation or force exists. The normal external load, F_n, is equal to the spring force produced by the compression springs. Hence, the entire model is in a force balance. The gas in the cylinder is compressed under the force of two compression springs and is in equilibrium. The compression deformation, x_i, of the two compression springs can be expressed as follows:

$$x_i = F_n/k_i \ (i = 1, 2).$$ (2)

In addition, F_n causes single-tooth elastic deformations of the pinion and gear. Therefore, their sum can be expressed as:

$$\sum_{i=1}^{2} x_i = F_n \left(\frac{1}{k_1} + \frac{1}{k_2} \right).$$ (3)

According to the relationship between k_i and k, $\frac{1}{k} = \frac{1}{k_1} + \frac{1}{k_2}$. Therefore, Eq. (3) can be simplified as:

$$\sum_{i=1}^{2} x_i = F_n/k.$$ (4)

Then, $x = F_n / k$, where x is the tooth pair's elastic deformation caused by F_n. Thus, $x = x_1 + x_2$.

Thermal expansion occurs owing to an increase in temperature. Furthermore, it is restricted by F_n. Therefore, an additional thermal load and thermal deformation are produced at the meshing point. This is equivalent to heating the cylinder continuously in the stiffness model. Consequently, the gas in the cylinder expands and disrupts the original equilibrium state until a new equilibrium state is established. At this instant, each spring in the model sustains a larger load and produce further deformation. These increments in load and deformation are the additional thermal load and temperature deformation of the system in the state of thermal expansion.
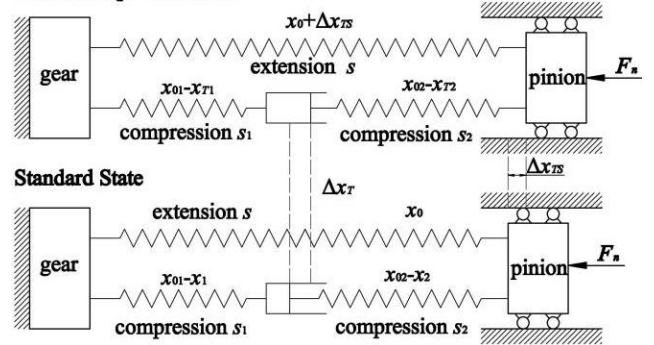

Fig. 1 Temperature stiffness model of gear pair in thermal expansion state

As shown in Fig. 1, the gas in the cylinder is heated and expanded. Thereby, the piston shifts to the right by Δx_T. The pinion shifts to the right to attain a new equilibrium state. The displacement of the pinion relative to the standard position is Δx_{TS}, which is the deformation of the extension spring. Corresponding to the gear system, Δx_{TS} is the temperature deformation increment of the tooth pair along the line of action in the thermal expansion state. Δx_T denotes the restricted expansion deformation of the tooth pair along the line of action. x_{T1} and x_{T2} are the coupling deformations along the line of action of the pinion and gear, respectively, at the contact point. The following relationship exists between the above deformations:

$$\Delta x_T = x_{T1} - x_1 + x_{T2} - x_2 + \Delta x_{TS}.$$ (5)

Then the coupling deformation, x_T along the line of action of the tooth pair can be calculated by Eq. (6).

$$x_T = x + \Delta x_{TS}.$$ (6)

x_{T1} and x_{T2} can be determined using Eq. (7) according to the force balance under thermal expansion conditions:

$$\begin{cases} x_{T1} = \dfrac{kx_T}{k_1} \\ x_{T2} = \dfrac{kx_T}{k_2} \end{cases}. \tag{7}$$

The normal temperature deformation increment of the tooth pair can be expressed as follows based on Eqs. (5–7):

$$\Delta x_{TS} = \frac{1}{2} \Delta x_T. \tag{8}$$

That is, in the thermal expansion state, the normal temperature deformation increment of the tooth pair is half of its normal restricted expansion deformation (also equal to the cylinder piston displacement). The magnitude of the piston displacement depends on the amount of external energy input, i.e., the energy variation, Q, caused by an increase in gear temperature. In this study, the increase in the elastic potential energy caused by the thermal expansion of the tooth profile in the free state was used to measure the energy variation caused by an increase in temperature of the system. Thus, the energy variation, Q caused by an increase in gear temperature can be determined using Eq. (9):

$$Q = \frac{1}{2} \sum_{i=1}^{2} k_i \Delta x_{pi}^2, \tag{9}$$

where: Δx_{pi} denotes the normal thermal expansion deformation of an individual tooth in the free state. The subscript $i = 1,2$ indicates the pinion or gear. The specific method for calculating Δx_{pi} is available in the literature [27].

The mechanical work W of the air cylinder during thermal expansion can be determined using Eq. (10):

$$W = \frac{1}{2} (F_n + F_n + k \Delta x_{TS}) \Delta x_T. \tag{10}$$

In accordance with the energy conservation of the system, the energy input from outside to the cylinder is equal to the mechanical work of the cylinder expressed in Eq. (11):

$$\frac{1}{2} \sum_{i=1}^{2} k_i \Delta x_{pi}^2 = \frac{1}{2} (F_n + F_n + k \Delta x_{TS}) \Delta x_T. \tag{11}$$

Based on Eqs. (8) and (11), the normal restricted expansion deformation (Δx_T), normal temperature deformation increment (Δx_{TS}), and normal coupling deformation (x_T) of the tooth pair can be determined by Eqs. (12–14), respectively:

$$\Delta x_T = \sqrt{4x^2 + 2(k_1 x_{p1}^2 + k_2 x_{p2}^2)/k} - 2x, \tag{12}$$

$$\Delta x_{TS} = \sqrt{x^2 + (k_1 x_{p1}^2 + k_2 x_{p2}^2)/(2k)} - x, \tag{13}$$

$$x_T = \sqrt{x^2 + (k_1 x_{p1}^2 + k_2 x_{p2}^2)/(2k)}. \tag{14}$$

Therefore, the normal single-tooth coupling deformation x_{T1}, x_{T2} can be expressed as:

$$\begin{cases} x_{T1} = \dfrac{k\sqrt{x^2 + (k_1 x_{p1}^2 + k_2 x_{p2}^2)/(2k)}}{k_1} \\ x_{T2} = \dfrac{k\sqrt{x^2 + (k_1 x_{p1}^2 + k_2 x_{p2}^2)/(2k)}}{k_2} \end{cases}. \tag{15}$$

The normal single-tooth temperature deformation increment Δx_{TS1}, Δx_{TS2} can be expressed as:

$$\begin{cases} \Delta x_{TS1} = x_{T1} - x_1 = \dfrac{k}{k_1} \Delta x_{TS} \\ \Delta x_{TS2} = x_{T2} - x_2 = \dfrac{k}{k_2} \Delta x_{TS} \end{cases}. \tag{16}$$

The temperature meshing stiffness k_T of the tooth pair under thermal expansion conditions can be expressed as follows according to the definition of temperature stiffness:

$$k_T = \frac{F_n}{x_T} = \frac{kx}{\sqrt{x^2 + (k_1 x_{p1}^2 + k_2 x_{p2}^2)/(2k)}}. \tag{17}$$

The single-tooth temperature stiffness k_{T1}, k_{T2} of the pinion and gear under thermal expansion conditions can be expressed as:

$$\begin{cases} k_{T1} = \dfrac{F_n}{x_{T1}} = \dfrac{k_1 x}{\sqrt{x^2 + (k_1 x_{p1}^2 + k_2 x_{p2}^2)/(2k)}} \\ k_{T2} = \dfrac{F_n}{x_{T2}} = \dfrac{k_2 x}{\sqrt{x^2 + (k_1 x_{p1}^2 + k_2 x_{p2}^2)/(2k)}} \end{cases}. \tag{18}$$

According to the definition of compliance, the temperature compliance δ_T of the meshing tooth pair in the state of thermal expansion can be expressed as:

$$\delta_T = \frac{x + \Delta x_{TS}}{F_n} = \delta + \delta_{TS}, \tag{19}$$

where: δ_{TS} denotes the compliance caused by Δx_{TS}, and $\delta_{TS} = \Delta x_{TS}/F_n$. This is known as the thermal expansion compliance of the tooth pair.

Similarly, the temperature compliance δ_{Ti} of a single tooth under thermal expansion conditions is obtained as expressed in Eq. (20). The subscript $i = 1, 2$ indicates the pinion or gear.

$$\delta_{Ti} = \frac{x_i + \Delta x_{TSi}}{F_n} = \delta_i + \delta_{TSi}, \tag{20}$$

where: δ_{TSi} signifies the compliance caused by Δx_{TSi}, and $\delta_{TSi} = \Delta x_{TSi}/F_n$. This is called the thermal expansion compliance of a single tooth.

Based on the relationship between stiffness and compliance, k_T and k_{Ti} can be given as Eqs. (21-22).

$$\frac{1}{k_T} = \delta_T = \delta + \delta_{TS} = \frac{1}{k} + \frac{1}{k_{TS}}, \tag{21}$$

$$\frac{1}{k_{Ti}} = \delta_{Ti} = \delta_i + \delta_{TSi} = \frac{1}{k_i} + \frac{1}{k_{TSi}}, \tag{22}$$

where: k_{TS} indicates the tooth pair's thermal expansion stiffness owing to Δx_{TS}, and k_{TSi} indicates the single tooth's thermal expansion stiffness owing to Δx_{TSi}, under the thermal expansion condition. The subscript $i = 1, 2$ indicates the pinion or gear.

To summarize, under the thermal expansion condition, the reciprocal of temperature meshing stiffness, $1/k_T$, of the tooth pair is the sum of the reciprocal of standard meshing stiffness, $1/k$, and expansion stiffness, $1/k_{TS}$, of the tooth pair. The reciprocal of single-tooth temperature stiffness, $1/k_{Ti}$, is the sum of the reciprocal of standard single-tooth stiffness, $1/k_i$, and single-tooth expansion stiffness, $1/k_{TSi}$. Just like a series connection of two springs.

3.2. Temperature stiffness in cold shrinkage state

When the beginning temperature of gears is lower than the standard temperature. The gear is in a state of cold shrinkage. Fig. 2 presents the tooth pair's temperature stiffness model in the cold shrinkage state.
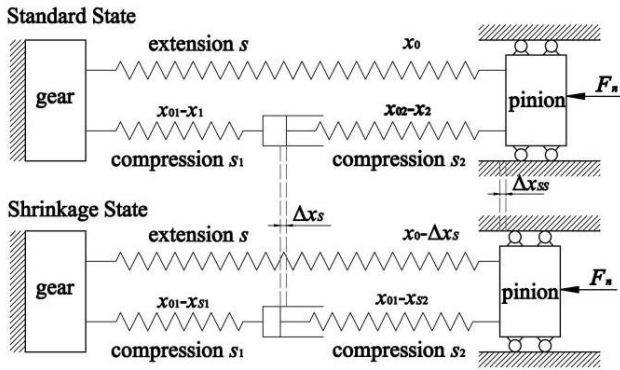

Fig. 2 Temperature stiffness model of gear in cold shrinkage state

As shown in Fig. 2, the gas in the cylinder contracts with a decrease in temperature. This causes the piston to shift to the left, and the displacement is, Δx_S. The pinion shifts to the left to attain a new equilibrium. The displacement of the pinion relative to the standard position is, Δx_{SS}. At present, the deformation, Δx_{SS}, of the extension spring is the normal increment in the tooth pair's temperature deformation in the shrinkage state. Δx_S denotes the tooth pair's normal shrinkage deformation.

However, in the cold shrinkage state, the shrinkage deformation direction at the contact point remains identical to that of the elastic deformation caused by external load. No additional load or deformation occur at the meshing point. As shown in Fig. 2, the length of the extension spring is reduced, and there is no tensile force. Consequently, the normal increment in the temperature deformation, Δx_{SS}, of the tooth pair is equal to the normal shrinkage deformation, Δx_S, of the tooth pair. The tooth pair's coupling deformation,

x_S, along the action line is a simple superposition of Δx_{SS} and x. That is:

$$\begin{cases} \Delta x_{SS} = \Delta x_S \\ \Delta x_{SSi} = \Delta x_{Si} \\ x_{Si} = x_i + \Delta x_{Si} \\ x_S = x + \Delta x_S \end{cases}, \tag{23}$$

where: Δx_{Si} indicates the normal shrinkage deformation of a single tooth. A detailed description of the calculation method is available in the literature [27]. Δx_{SSi} denotes the normal temperature deformation increment of a single tooth in the cold shrinkage state. x_{Si} signifies the normal single-tooth coupling deformation in the cold shrinkage state. The subscript $i = 1,2$ indicates the pinion or gear.

Based on the definition of temperature stiffness, the temperature meshing stiffness, k_S, and single-tooth temperature stiffness, k_{Si}, in the cold shrinkage state can be expressed as:

$$\begin{cases} k_S = F_n / (x + \Delta x_S) \\ k_{Si} = F_n / (x_i + \Delta x_{Si}) \end{cases}. \tag{24}$$

According to the definition of compliance, the temperature compliance, δ_S, of the tooth pair and single-tooth temperature compliance, δ_{Si}, in the cold shrinkage state can be expressed as:

$$\begin{cases} \delta_S = (x + \Delta x_S)/F_n = \delta + \delta_{SS} \\ \delta_{Si} = (x_i + \Delta x_{Si})/F_n = \delta_i + \delta_{SSi} \end{cases}, \tag{25}$$

where: δ_{SS} is the compliance caused by Δx_{SS}, and $\delta_{SS} = \Delta x_{SS} / F_n$. This is called the shrinkage compliance of the tooth pair. δ_{SSi} is the compliance caused by Δx_{SSi}, and $\delta_{SSi} = \Delta x_{SSi}/ F_n$. This is called the shrinkage compliance of a single tooth.

On the basis of the relationship between the compliance and stiffness, the k_S and k_{Si} is given as Eq. (26).

$$\begin{cases} \dfrac{1}{k_S} = \delta_S = \delta + \delta_{SS} = \dfrac{1}{k} + \dfrac{1}{k_{SS}} \\ \dfrac{1}{k_{Si}} = \delta_{Si} = \delta_i + \delta_{SSi} = \dfrac{1}{k_i} + \dfrac{1}{k_{SSi}} \end{cases}, \tag{26}$$

where: k_{SS} indicates the tooth pair's shrinkage stiffness owing to Δx_{SS} under the contraction condition, and k_{SSi} denotes the single tooth shrinkage stiffness owing to Δx_{SSi} under the contraction condition. The subscript $i = 1, 2$ signifies the pinion or gear.

From Eq. (26), in the cold shrinkage state, the reciprocal of temperature meshing stiffness, $1/k_S$, of the tooth pair is the sum of the reciprocal of standard meshing stiffness, $1/k$, and the reciprocal of shrinkage stiffness, $1/k_{SS}$, of the tooth pair. The reciprocal of single tooth temperature stiffness, $1/k_{Si}$, is the sum of the reciprocal of standard single tooth stiffness, $1/k_i$, and the reciprocal of single tooth shrinkage stiffness, $1/k_{SSi}$. Just like a series connection of two springs.

Based on the above analysis, the temperature meshing stiffness, c_0 and single tooth temperature stiffness,

c_i, of the gear in the full temperature range can be expressed as:

$$c_0 = \begin{cases} \dfrac{kk_{TS}}{k + k_{TS}} & t \geq t_0 \\[2ex] \dfrac{kk_{SS}}{k + k_{SS}} & t < t_0 \end{cases}, \qquad (27)$$

$$c_i = \begin{cases} \dfrac{k_i k_{TSi}}{k_i + k_{TSi}} & t \geq t_0 \\[2ex] \dfrac{k_i k_{SSi}}{k_i + k_{SSi}} & t < t_0 \end{cases}, \qquad (28)$$

where: t and t_0 are the actual and standard temperature of the gear, respectively. Based on Eqs. (27–28), in the full temperature range, both temperature meshing stiffness and sin-gle-tooth stiffness is less than the corresponding standard stiffness. Consequently, when the initial temperature of the gear below the standard temperature, the temperature meshing stiffness and single-tooth stiffness first increase and then decrease with gradual increase in the temperature. That is, the stiffness of the gear displays a "low–high–low" variation with an increase in temperature.

4. Case analysis and discussion

Two different cases are presented in Table 1. The gear pair's standard temperature is 30 °C. The temperature of the meshing tooth surfaces for both pinion and gear is 70 °C under the thermal expansion condition, whereas it is 10 °C under the contraction condition. The non-uniform temperature distribution along the meshing line is omitted. The material linear expansion coefficient is 1.13×10^{-5} °C^{-1}. The gear's standard stiffness calculation method is presented in the literature [29].

Table 1

Fundamental parameters of gear pair

	Module m, mm	Tooth number z_1, z_2	Pressure angle α, °	Shift coefficient x_1, x_2	Addendum coefficient h_a^*	Tip clearance coefficient c^*
Gear pair I	3.0	27/35	20	0, 0	1.0	0.25
	Face width b, mm	Standard center distance a, mm	Height of tooth h_a, mm	Pitch radius r_1, r_2, mm	Tip radius r_{a1}, r_{a2}, mm	Base radius r_{b1}, r_{b2}, mm
	25	93	6.75	40.5, 52.5	43.5, 55.5	38.06, 49.33
Gear pair II	Module m, mm	Tooth number z_1, z_2	Pressure angle α, °	Shift coefficient x_1, x_2	Addendum coefficient h_a^*	Tip clearance coefficient c^*
	4.5	16/24	20	0.8532, -0.5	1.0	0.25
	Face width b, mm	Standard center distance a, mm	Height of tooth h_a, mm	Pitch radius r_1, r_2, mm	Tip radius r_{a1}, r_{a2}, mm	Base radius r_{b1}, r_{b2}, mm
*	20	91.5	10.04	36.60, 54.90	44.25, 56.16	33.83, 50.74

To accurately represent the distribution of each parameter along the line of action, the positional coordinates of the arbitrary contact points, K, on the meshing line are represented by the normalized coordinate, Γ_K. From Fig. 3, the line of action is considered as the coordinate axis, point C is the coordinate origin, and the direction of point C to point N_1 is the negative direction. Therefore, Γ_K can be defined as $\Gamma_K = \dfrac{\overline{N_1K} - \overline{N_1C}}{\overline{N_1C}} = \dfrac{\tan\alpha_K}{\tan\alpha_C} - 1$, where α_C is the pressure angle of the pitch point C, and α_K is the pressure angle of point K on the pinion.
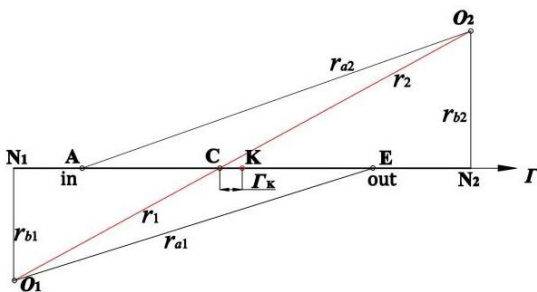

Fig. 3 Normalized coordinates of the line of action. A – meshing-in point; C – pitch point; E – meshing-out point; K – arbitrary meshing point in the entire meshing region; N_1 – ideal meshing-in point; N_2 – ideal meshing-out point

Fig. 4 presents the distribution curves of the temperature meshing stiffness and single-tooth temperature compliance along the line of action.

As shown in Fig.4, δ_S denotes the temperature compliance of the tooth pair in the cold shrinkage state; k_S denotes the temperature meshing stiffness of the tooth pair in the cold shrinkage state; δ_{Si} denotes the temperature compliance of single-tooth in the cold shrinkage state; δ_T is the temperature compliance of the tooth pair in the thermal expansion state; k_T is the temperature meshing stiffness of the tooth pair in the thermal expansion state; δ_{Ti} denotes the temperature compliance of single-tooth in the thermal expansion state; δ denotes the compliance of the tooth pair in the standard state; k represents the meshing stiffness of the tooth pair in the standard state; δ_{Ti} is the compliance of single-tooth in the standard state; the subscript $i = 1, 2$ signifies the pinion or gear.

From Fig. 4, both on the conditions of thermal expansion and cold shrinkage, the single tooth temperature compliance is larger than the single-tooth standard compliance in the whole contact region. Under different conditions, Tables 2 and 3 list the stiffness data of the gear at the key points. From Fig. 4 and Table 2, in the full temperature range, the single-tooth temperature stiffness decreases compared to the single-tooth standard stiffness in the whole contact region. The decrement in stiffness increases from the tip to the root of the tooth. Meanwhile, under the thermal expansion condition, similar results are presented in the literature [27] (Figs. 3, a and 10, a in the literature [27]). Significantly, the unit tooth width stiffness was used in that study. Thus, the stiffness value obtained in the mentioned literature is approximately 40 times than that obtained in the current study (the tooth width study is 25 mm).

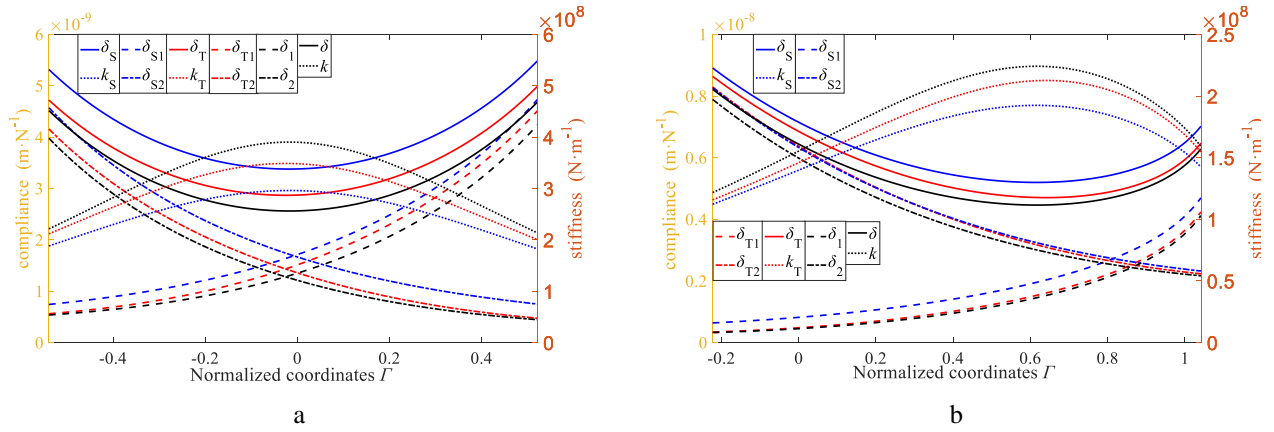<center>a</center> <center>b</center>

Fig. 4 Distribution curves of temperature stiffness and compliance along the line of action: a) distribution curves – gear pair I; b) distribution curves – gear pair II

<div align="right">Table 2</div>

<center>Single-tooth stiffness data of gear at key points under different conditions</center>

Key points		Stiffness of pinion (× 10^8 N/m)			Stiffness of gear (× 10^8 N/m)		
		Meshing-in (Root of the tooth)	Pitch	Meshing-out (Tip of the tooth)	Meshing-in (Tip of the tooth)	Pitch	Meshing-out (Root of the tooth)
Gear pair I	Standard	18.5940	7.4045	2.3619	2.5141	8.2403	22.3810
	Expansion	17.9410	6.7564	2.2383	2.4759	7.4968	21.2100
	Difference	-0.6526	-0.6481	-0.1236	-0.0882	-0.7435	-1.1717
	Shrinkage	13.4620	5.8402	2.1143	2.1869	5.9959	13.3090
	Difference	-5.1322	-1.5642	-0.2476	-0.3272	-2.2444	-9.0726
Gear pair II	Standard	30.6230	22.0610	2.4278	1.2675	1.6713	4.6155
	Expansion	29.5070	21.0500	2.3929	1.2213	1.5947	4.5493
	Difference	-1.1160	-1.0110	-0.0348	-0.0419	-0.0766	-0.0662
	Shrinkage	15.6580	12.1930	2.1293	1.2093	1.5807	4.3053
	Difference	-14.9660	-9.8682	-0.2985	-0.0582	-0.0906	-0.3102

<div align="right">Table 3</div>

<center>Meshing stiffness data of gear at key points under different conditions</center>

Key points		Meshing-in	Pitch	Meshing-out	Max
Meshing stiffness of gear pair I (× 10^8 N/m)	Standard	2.2147	3.9000	2.1365	3.9029
	Expansion	2.1370	3.5481	2.0246	3.5531
	Difference	-0.0777	-0.3519	-0.1118	-0.3498
	Shrinkage	1.8813	2.9585	1.8245	2.9602
	Difference	-0.3334	-0.9415	-0.3120	-0.9427
Meshing stiffness of gear pair II (× 10^8 N/m)	Standard	1.2171	1.5536	1.5909	2.2412
	Expansion	1.1728	1.4824	1.5681	2.1522
	Difference	-0.0444	-0.0712	-0.0228	-0.0890
	Shrinkage	1.1226	1.3993	1.4247	1.9242
	Difference	-0.0946	-0.1543	-0.1662	-0.3170

By combining Fig. 4 and Table 3, in the full temperature range, the temperature meshing stiffness is noticed to be less than the standard meshing stiffness in the whole contact region. The stiffness reductions at the meshing-in and -out points are smaller than those nearby the pitch point and the similar results can be found in the literature [27]. For gear pair I without a tooth profile shift, the largest reduction occurs near the pitch point. For gear pair II with a tooth profile shift, the meshing point corresponding to the maximum stiffness reduction is far away from the pitch point. That is, if the pitch point shifts toward the meshing-in point after tooth profile shift, the meshing point corresponding to the maximum stiffness reduction shifts toward the meshing-out point.

Fig. 5 shows the influence of temperature on the gear stiffness through the distribution curves of the temperature meshing stiffness along the line of action at different temperatures. The figure shows that the temperature meshing stiffness first increases and then decreases with the increase in temperature, and the maximum stiffness is obtained at the standard temperature.

During the contact of the gear, its bulk temperature is mainly determined by the external load. In addition, an apparent temperature gradient exists. In this study, a thermal analysis model of the gear was established using FEM to investigate the influence of temperature on gear stiffness more accurately. Fig. 6a shows the temperature result. Subsequently, the temperature data of each node on the contact surface were extracted. Thereafter, the distribution curve of temperature along the line of action at the middle of the tooth width was obtained by employing the data fitting method, as shown in Fig. 6b. The detailed modelling and

analysis methods are available in the literature [29]. Table 4 lists the working conditions, materials, and lubrication parameters required for the thermal analysis of the gears.
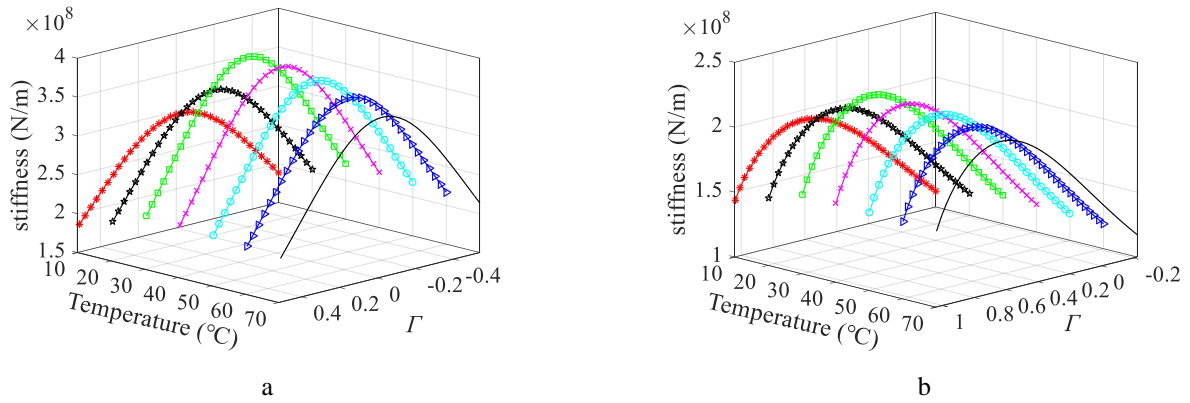

a

b

Fig. 5 Temperature meshing stiffness of tooth pair under different temperatures: a) gear pair I; b) gear pair II

Table 4

Parameters required for thermal analysis of gears [29]

	Power P, kW	Rotation rate n_1, rpm	Density ρ, kg·m^{-3}	Poisson's ratio υ	Young's modulus E, Pa
Load & material parameters	80	2000	7850	0.3	2.06×10^{11}
	Thermal conductivity λ, W·(m·K)$^{-1}$		Thermal capacity c, J·(kg·K)$^{-1}$		
	46		465		
Lubricant oil parameters	Lubricant model		Density ρ_o, kg·m^{-3}	Thermal conductivity λ_o, W·(m·K)$^{-1}$	
	SCH632		870	0.14	
	Thermal capacity C_o, J·(kg·K)$^{-1}$		Kinematic viscosity υ_o, cst	Oil operating temperature t_{oot}, °C	
	2000		320 (40 °C) / 38.5 (100 °C)	60	

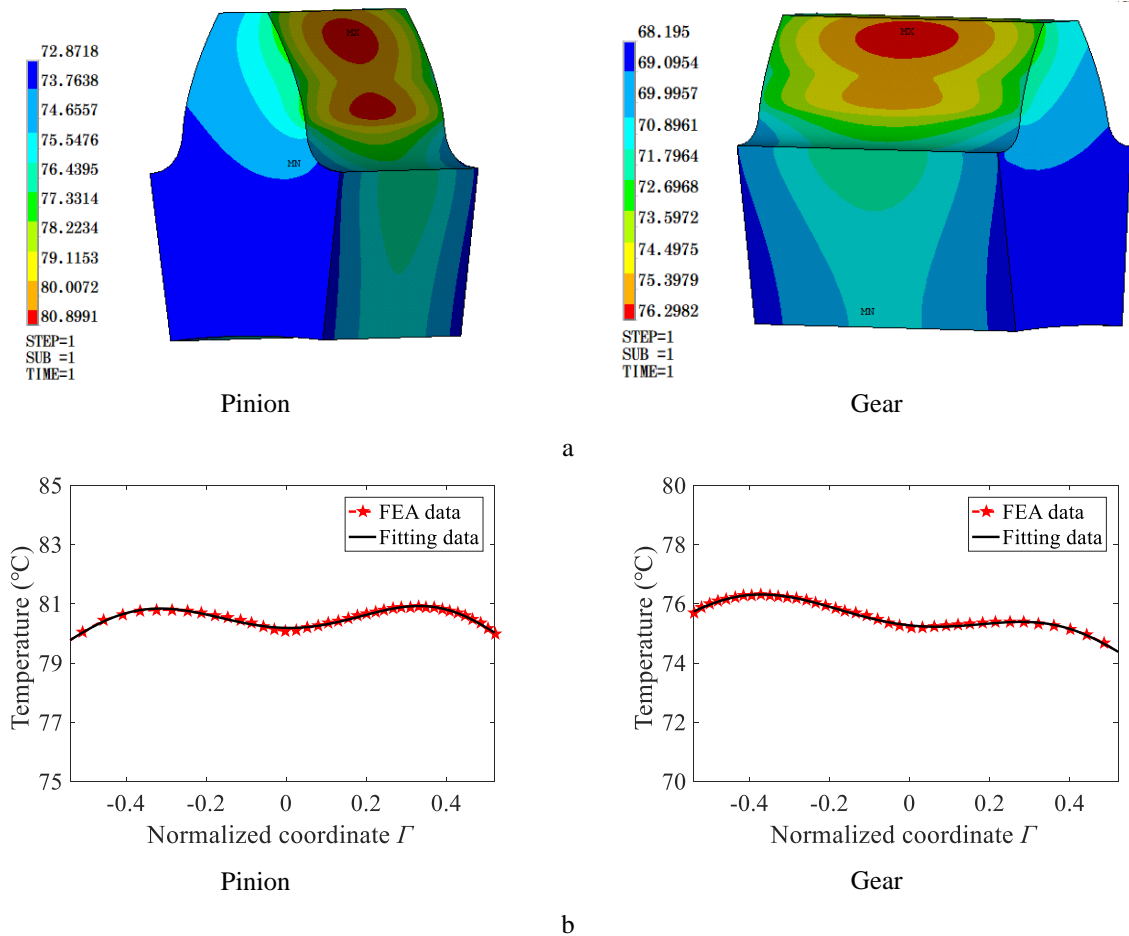Pinion

Gear

a

Pinion

Gear

b

Fig. 6 The bulk temperature for gear pair I: a) single tooth bulk temperature of gear pair I; b) bulk temperature distribution curve at the middle of the tooth width – gear pair I

The fitting data in Fig. 6b was used to calculate the temperature stiffness of the gear. Then, the actual temperature stiffness of the gear could be obtained. Meanwhile, the mean value (pinion: 80.48 °C, gear: 75.54 °C) of the bulk temperature was also used and the non-uniform distribution of temperature along the line of action was omitted. Then the actual temperature stiffness results are shown in Fig. 7.

From Fig. 7, the temperature stiffness obtained using the average temperature was less than that obtained using the bulk temperature. However, the distribution of the stiffness along the line of action was consistent. Therefore, the average temperature could be used to estimate the temperature stiffness of the gear.

5. Verification of temperature stiffness model

The correctness of the proposed model under the condition of thermal expansion was verified by comparing the meshing stiffness with that of the literature [27].

It is challenging to directly obtain the stiffness of gears at different temperatures using an experimental method. In this work, an indirect verification method based on the relationship between the stiffness and vibration natural frequency of the system was proposed. The fundamental concept of the experiment is shown in Fig. 8. In this study, the natural frequency at different temperatures was obtained. Thereafter, the variation of the natural frequency with temperature was used to indirectly verify the correctness of the proposed model.

As presented in Fig. 8, the key to verify the correctness of the proposed model is to identify a method to obtain the beat vibration signal of the system. Referring to the literature [30], the gear vibration test platform was established. The parameters of the experimental gear pair were consistent with gear pair II presented in Table 1. The experimental system exhibited a beat phenomenon at 900 rpm. The experiment was conducted in winter in northern China to obtain the gear vibration signal under cold contraction conditions. Table 5 lists the temperature and load parameters associated with the experiments.
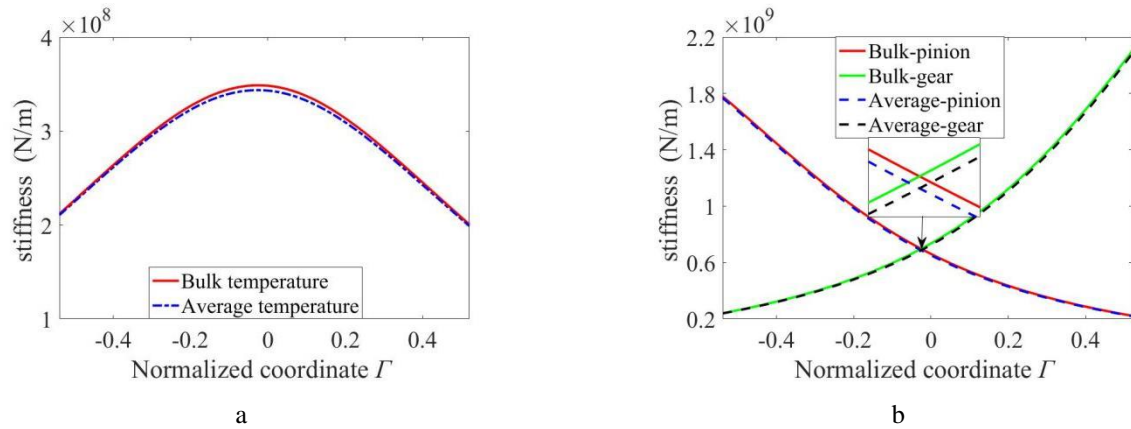

Fig. 7 Temperature meshing stiffness under different temperatures: a) meshing stiffness; b) single-tooth stiffness
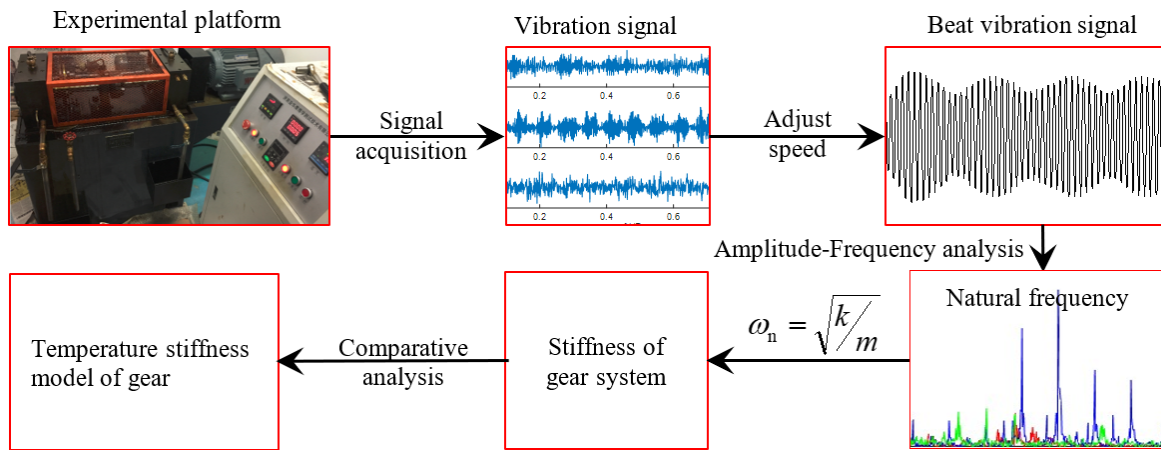

Fig. 8 The basic ideas for the experimental validation

Table 5

Experimental conditions

Initial temperature, °C				Load, N/m		Rotational speed of pinion, rpm
Ambient	Lubricating oil	Pinion	Gear	Level I	Level II	
5.2	9.2	8.4	8.3	14	138	900

During the gear contact process, the bulk temperature of the gear increases gradually owing to the friction heat. Therefore, the system beat vibration signal varies with variation in temperature. In the present experiment, the vibration test lasted for 20 min at a rotational speed of 900 rpm. The vibration signal and temperature of the system were obtained using a wireless acceleration sensor and temperature sensor, respectively. The system temperatures at different times under different load conditions are listed in Table 6.

From Table 6, the system temperature first increased rapidly with time, gradually after a certain period, and finally tended to be constant. The vibration signals of the 3rd, 5th, and 10th min was extracted from the 20 min vibration signal for performing a comparative analysis. Then the system natural frequencies at different temperatures were obtained. The system vibration acceleration-frequency characteristic curve is presented in Fig. 9.

Table 6

System temperature data at different times

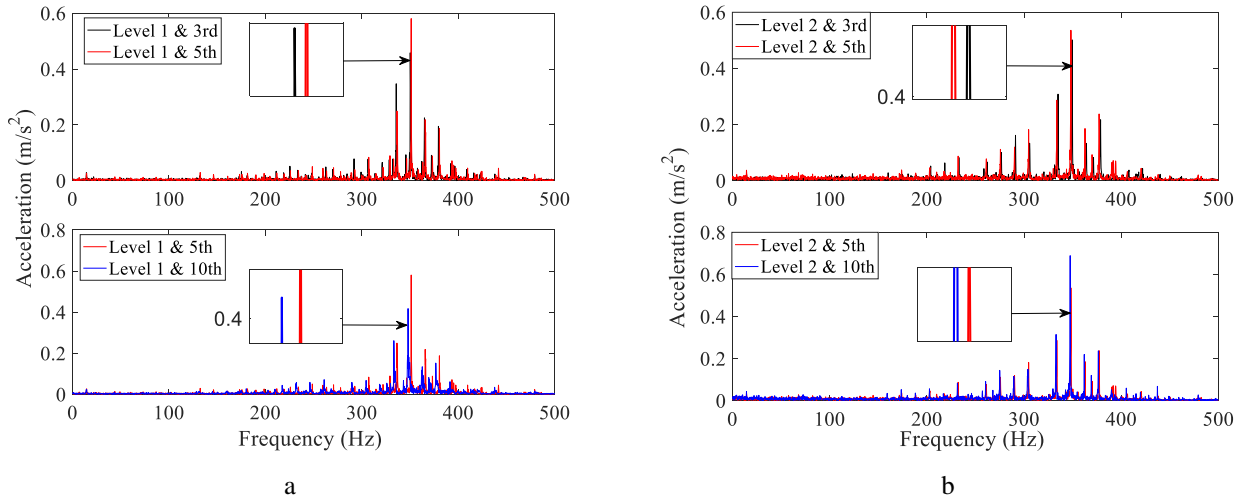| Time, min		1st	3rd	5th	7th	9th	10th	12th	14th	16th	18th	20th
Temperature, °C	Level 1	13.5	18.0	23.8	26.8	30.3	32.8	36.2	37.4	38.2	39.8	40.2
	Level 2	31.0	32.3	35.6	37.9	41.9	42.7	44.4	46.0	47.9	49.4	50.7

Fig. 9 The system vibration acceleration-frequency characteristic curve: a) load level I; b) load level II

From Table 6 and Fig. 9a, on load level I, the system beginning temperature below the standard temperature under the condition of. The natural frequencies at the 3rd and 10th min is less than that at the 5th min. That is, the system natural frequency first increases and then decreases with the increase in temperature. It displays a "low–high–low" variation. This is consistent with the trend of the gear temperature stiffness vs. temperature obtained by from the proposed stiffness model.

Based on Table 6 and Fig. 9b, on load level II, the system beginning temperature is higher than the standard temperature. The natural frequency at the 3rd min is larger than that at the 5th min, which is larger than that at the 10th min. That is, the natural frequency of the system decreases with an increase in temperature. Consequently, the stiffness of the system also decreases with an increase in temperature owing to the relationship between stiffness and natural frequency. This is consistent with the trend of the temperature stiffness vs. temperature in the thermal expansion state. Thus, the correctness of the gear temperature stiffness model was verified by the above experimental study.

6. Conclusion

To conclude, the effect of temperature on gear stiffness is investigated in the full temperature range in this paper. The concept of temperature stiffness is proposed. Thereafter, the temperature stiffness model of the gear is established based on energy conservation. A general formula for calculating the gear temperature stiffness is derived, and a verification experiment is carried out. The observations are summarized below:

1. In the full temperature range, the reciprocal of temperature stiffness of the gear is the sum of the reciprocal of gear standard stiffness and the expansion (or shrinkage) stiffness of the gear. Just like a series connection of two springs.

2. In the full temperature range, the gear's temperature stiffness is less than the standard stiffness. The single-tooth stiffness reduction increases from the root to the tip. The reduction in meshing stiffness at the pitch point is bigger than that at the meshing-in and -out points.

3. When the gear beginning temperature is below the standard temperature, the gear temperature stiffness first increases and then decreases with the increase in gear temperature. That is, it displayed a "low–high-low" variation.

Acknowledgments

Conflict of interest

The authors declare that they have no conflict of interest.

Author contributions statement

All the authors contributed to the study conception and design. Material preparation, data collection, and analysis were performed by Yanbing He and Haibo Yang. The first draft of the manuscript was written by Yanbing He, and all the authors provided their feedback on previous versions of the manuscript. All the authors have read and approved the final manuscript.

Reference

1. **Fernandez del Rincon, A.; Viadero, F.; Iglesias, M.;** et al. 2013. A model for the study of meshing stiffness in spur gear transmissions, Mechanism and Machine Theory 61: 30-58.
http://dx.doi.org/10.1016/j.mechmachtheory.2012.10.008.

2. **Chen, Z. G.; Shao, Y. M.** 2013. Mesh stiffness of an internal spur gear pair with ring gear rim deformation, Mechanism and Machine Theory 69: 1-12.
http://dx.doi.org/10.1016/j.mechmachtheory.2013.04.017.

3. **Liang, X. H.; Zhang, H. S.; Zuo, M. J.;** et al. 2018. Three new models for evaluation of standard involute spur gear mesh stiffness, Mechanical Systems and Signal Processing 101: 424-434.
http://dx.doi.org/10.1016/j.ymssp.2017.09.005.

4. **Tang, X. L.; Zou, L.; Yang, W.;** et al. 2018. Novel mathematical modelling methods of comprehensive mesh stiffness for spur and helical gears, Applied Mathematical Modelling 64: 524-540.
https://doi.org/10.1016/j.apm.2018.08.003.

5. **Feng, M. J.; Ma, H.; Li, Z. W.;** et al. 2018. An improved analytical method for calculating time-varying mesh stiffness of helical gears, Meccanica 53(4-5): 1131-1145.
https://dx.doi.org/10.1007/s11012-017-0746-6.

6. **Yang. Y.; Wang, J. X.; Zhou, Q. H.;** et al. 2018, Mesh stiffness modeling considering actual tooth profile geometry for a spur gear pair, Mechanics & Industry 19(3): 306.
https://doi.org/10.1051/meca/2018026.

7. **Feng, S.; Chang, L. H.; He, Z. X.** 2020. A hybrid finite element and analytical model for determining the mesh stiffness of internal gear pairs, Journal of Mechanical Science and Technology 34(6): 2477-2485.
http://doi.org/10.1007/s12206-020-0523-7.

8. **Tang, J. Y.; Pu, T. P.** 2011. Spiral bevel gear meshing stiffness calculations based on the finite element method, Journal of Mechanical Engineering 47(11): 23-29 (in Chinese).
http://dx.doi.org/10.3901/JME.2011.11.023.

9. **Verma, J. G.; Kumar, S.; Kankar, P. K.** 2018. Crack growth modeling in spur gear tooth and its effect on mesh stiffness using extended finite element method, Engineering Failure Analysis 94: 109-120.
http://dx.doi.org/10.1016/j.engfailanal.2018.07.032.

10. **Karpat, F.; Dogan, O.; Yuce, C.;** et al. 2017. An improved numerical method for the mesh stiffness calculation of spur gears with asymmetric teeth on dynamic load analysis, Advances in Mechanical Engineering 9(8): 1-12.
https://doi.dox.org/10.1177/1687814017721856.

11. **Cooley, C. G.; Liu, C. G.; Dai, X.** 2016. Gear tooth mesh stiffness: a comparison of calculation approaches, Mechanism and Machine Theory 105: 540-553.
http://dx.doi.org/10.1016/j.mechmachtheory.2016.07.021.

12. **Karpat, F.; Yuce, C.; Dugan, O.** 2020. Experimental measurement and numerical validation of single tooth stiffness for involute spur gears, Measurement 150: 107043.
https://doi.org/10.1016/j.measurement.2019.107043.

13. **Raghuwanshi, N. K.; Parey, A.** 2018. Experimental measurement of mesh stiffness by laser displacement sensor technique, Measurement 128: 63-70.
https://doi.org/10.1016/j.measurement.2018.06.035.

14. **Saxena, A.; Parey, A.; Chouksey, M.** 2016. Time varying mesh stiffness calculation of spur gear pair considering sliding friction and spalling defects, Engineering Failure Analysis 70: 200-211.
http://dx.doi.org/10.1016/j.engfailanal.2016.09.003.

15. **Ma, H.; Li, Z. W.; Feng, M. J.;** et al. 2016. Time-varying mesh stiffness calculation of spur gears with spalling defect, Engineering Failure Analysis 66:166-176.
http://dx.doi.org/10.1016/j.engfailanal.2016.04.025.

16. **Cui, L. L.; Liu, T. T.; Huang, J. F.;** et al. 2019. Improvement on meshing stiffness algorithms of gear with peeling, Symmetry-basel 11(5): 609.
http://dx.doi.org/10.3390/sym11050609.

17. **Luo, Y.; Baddour, N.; Han, G. S.;** et al. 2018. Evaluation of the time-varying mesh stiffness for gears with tooth spalls with curved-bottom features, Engineering Failure Analysis 92: 430-442.
https://doi.org/10.1016/j.engfailanal.2018.06.010.

18. **Wang, Q. B.; Chen, K. K.; Zhao, B.;** et al. 2018. An analytical-finite-element method for calculating mesh stiffness of spur gear pairs with complicated foundation and crack, Engineering Failure Analysis 94: 339-353.
https://doi.org/10.1016/j.engfailanal.2018.08.013.

19. **Jiang, H. J.; Liu, F. H.** 2020. Mesh stiffness modelling and dynamic simulation of helical gears with tooth crack propagation, Meccanica 55(6): 1215-1236.
https://doi.org/10.1007/s11012-020-01159-5.

20. **Jiang, H. J.; Liu, F. H.** 2019. Analytical models of mesh stiffness for cracked spur gears considering gear body deflection and dynamic simulation, Meccanica 54(11-12): 1889-1909.
https://doi.org/10.1007/s11012-019-01053-9.

21. **Chen, Z. G.; Zhai, W. M.; Shao, Y. M.** 2016. Analytical model for mesh stiffness calculation of spur gear pair with non-uniformly distributed tooth root crack, Engineering Failure Analysis 66: 502-514.
http://dx.doi.org/10.1016/j.engfailanal.2016.05.006.

22. **Chen, Z. G.; Zhai, W. M.; Shao, Y. M.;** et al. 2016. Mesh stiffness evaluation of an internal spur gear pair with tooth profile shift, Science China-Technological Sciences 59(9): 1328-1339.
http://dx.doi.org/10.1007/s11431-016-6090-6.

23. **Liang, X. H.; Zhang, H. S.; Liu, L. B.;** et al. 2016. The influence of tooth pitting on the mesh stiffness of a pair of external spur gears, Mechanism and Machine Theory 106: 1-15.
http://dx.doi.org/10.1016/j.mechmachtheory.2016.08.005.

24. **Cheng, G.; Xiao, K.; Wang, J. X.;** et al. 2020. Calculation of gear meshing stiffness considering lubrication, Journal of Tribology-Transactions of the ASME 142(3): 031602.
http://dx.doi.org/10.1115/1.4045499.

25. **Wang, Q. B.; Zhao, B.; Fu, Y.;** et al. 2018, An improved time-varying mesh stiffness model for helical gear pairs considering axial mesh force component, Mechanical Systems and Signal Processing 106: 413-429.
https://doi.org/10.1016/j.ymssp.2018.01.012.

26. **Gou, X. F.; Qi, C. J.; Chen, D. L.** 2015, Nonlinear dynamic modelling and analysis of gear system with tooth

contact temperature, Journal of Mechanical Engineering 51: 71-77 (in Chinese).

http://dx.doi.org/10.3901/JME.2015.11.071.

27. **Luo, B.; Li, W.; Fu, C. M.;** et al. 2020. Investigation of the thermal stiffness and thermal tooth profile modification of spur gears, Journal of the Brazilian Society of Mechanical Sciences and Engineering 42: 150.

https://doi.org/10.1007/s40430-020-2234-5.

28. **Lin, T. J.; Zhao, Z. R.; Jiang, F. Y.** et al. 2020. An analytic algorithm of time-varying mesh stiffness of helical gears considering temperature effect, Journal of Hunan University (Natural Sciences) 47(2): 6-13 (in Chinese).

https://doi.org/10.16339/j.cnki.hdxbzkb.2020.02.002.

29. **Luo, B.; Li, W.** 2017. Influence factors on bulk temperature field of gear, Proceedings of the Institution of Mechanical Engineers Part J: Journal of Engineering Tribology 231(8): 953–964.

https://doi.org/10.1177/1350650116684275.

30. **Luo, B.; Li, W.** 2019. Experimental study on thermal dynamic characteristics of gear transmission system, Measurement 136: 154-162.

https://doi.org/10.1016/j.measurement.2018.12.066.

Y. B. He, H. B. Yang

NOVEL MESHING STIFFNESS MODEL FOR SPUR GEAR PAIRS CONSIDERING THE TEMPERATURE EFFECT

S u m m a r y

This work studied the effect of temperature on gear stiffness in the full temperature range which contained thermal expansion and cold shrinkage. Considering the temperature effect, a meshing stiffness model for spur gear pairs in the full temperature range was established based on the conservation of energy. The general calculation formula for the gear pair's temperature meshing stiffness in the full temperature range was derived. The influence of addendum modification and gear temperature distribution on gear stiffness was studied. Thereafter, the proposed model was verified experimentally. The results revealed that the temperature stiffness was smaller than the standard stiffness of the gears in the full temperature range. When the temperature of the gears increased from an initial temperature, which was lower than the standard temperature, the temperature stiffness of the gear first increased and then decreased. Moreover, the obtained results could provide theoretical support for an accurate dynamic analysis of gear transmission systems in the full temperature range.

Keywords: spur gear pairs; meshing stiffness model; temperature effect; full temperature range; conservation of energy.